JOURNAL OF MATERIALS SCIENCE 20 (1985) 3453–3461

Eutectoid transformations and precipitation in high carbon tool steels

J. D. B. DE MELLO*, S. HAMAR-THIBAULT, M. DURAND-CHARRE
Institut National Polytechnique de Grenoble, ENSEEG LTPCM, LA 29 BP 75 Domaine Universitaire, 38400 Saint Martin d'Hères, France

Delta ferrite undergoes some rather complex solid-state transformations during solidification and cooling. These have been investigated in a series of alloyed high carbon steels. Solidification paths have been determined using the quenching during differential thermal analysis method (QDTA). The different phases produced were identified by scanning and transmission electron microscopy and were analysed by electron probe microanalysis. Four different types of transformation were identified: solid state precipitation, cellular precipitation, delta eutectoid transformation and plate formation followed by two further precipitation reactions. The latter transformation results in the development of very hard and complex structures in which four phases are intimately associated. An explanation has been proposed for the mechanism of their formation.

1. Introduction

The choice of wear resistant materials is based mainly on mechanical performance and hardness is often considered as an important property for high abrasion resistance. However the correlation between bulk hardness and abrasion resistance is verified only for certain types of steels and possibly cast-irons [1]. The determining factors are carbon content and the corresponding microstructure. Carbon and alloying elements induce the formation of so-called special carbides which are complex chromium-, molybdenum-, vanadium- and iron-carbides. Incorporating large amounts of solidification carbides into the structure of the alloy is therefore an excellent way to improve abrasion resistance [2].

The good behaviour due to the hard carbides may be either enhanced or lost according to the state of the matrix supporting them. A soft matrix containing ferrite or pearlite will leave the particles of carbides to be dug out or broken before removal. In order to obtain the optimum combination of abrasion resistance and cost, alloys containing carbides in a predominantly martensitic matrix have been investigated. In a previous study of such alloys [3], we have observed very different structures for rather similar compositions. In these alloys the solid-state transformations ocurring are the formation of martensite, bainite and pearlite. These classical transformations are well known and described by the TTT curves [4]. They concern only alloys which develop an austenitic structure either during solidification or when heat treated. Amongst the cast-irons containing about 1 wt % carbon another series may be distinguished. These are the alloys in which delta-ferrite is formed. Delta-ferrite undergoes during cooling complex transformations: delta-eutectoid formation, cellular precipitation and formation of plate-like structures, as has been shown for 17% chromium stainless steels by Castro and Tricot [5]. These transformations are not very well defined and often misunderstood. As a general rule the transformation concerns just a small

**Present address*: Professor at Universidade Federal de Uberlandia, Depto-Fisica e Materiaïs, campus Sta Monica, Uberlandia M6, Brazil.

0022–2461/85 $03.00 + .12

proportion of the matrix, e.g. the rim of the grain. Their influence on the properties is consequently limited. Nevertheless these transformations may be responsible for small discontinuities which we have observed on the differential thermal analysis (DTA) thermograms and also for some of the unusual dilatometric effects reported by Maratray and Poulalion [6]. In practice these steels or cast-irons are often used in the as-cast state without any heat treatment; consequently the importance of the structural effect is evident and a good understanding of all the solid state transformations occurring within the matrix is necessary.

As the first step, the determination of the solidification paths should be carried out in order to understand the microstructure resulting from the formation of the successive phases during the solidification. This could be done using the methods of QDTA (quenching during the differential thermal analysis process) previously developed [7]. The purpose of the present paper is to show how, from a knowledge of the solidification and transformation mechanisms, the microstructure of the alloys at the end of the cooling process can be understood.

2. Experimental procedure

Eight alloys were investigated, the compositions of which are shown in Table I. DTA was performed on specimens of about 2 g in order to determine the phase transformation temperatures. In addition, solidification occurring under controlled conditions in the DTA furnace was monitored so that the specimen could be quenched at the precise moment at which either the liquidus surface or another transformation occurred. This technique, QDTA, in which the solid–liquid interface configuration is frozen-in by rapid cooling, enables the solidification sequence to be determined. Phase analyses were carried out on an electron microprobe with application of a *ZAF* correction programme, where *Z* is the atomic number, *A* the absorption and *F* the fluorescence. In the case of phases present in the form of fine particles, semi-quantitative analyses were also performed on a scanning electron microprobe (JSM 35) equipped with an X-ray dispersive detector.

TABLE I Composition of the alloys (Fe balance)

Alloy	Alloy composition (wt %)					
	C	Cr	Mn	Mo	Si	Ni
A	1.66	15.8	2.8	0.09	0.12	–
B	1.72	16.0	1.7	2.98	0.22	–
C	1.65	16.0	1.0	3.20	0.56	–
D	0.86	23.8	–	–	1.90	2.10
E	0.87	16.0	0.7	2.80	0.31	–
F	1.32	13.7	1.7	2.98	0.22	–
G	0.92	11.3	0.7	2.95	0.33	–
H	0.79	32.5	1.1	3.01	0.55	–

Phase identification was made by transmission electron microscopy (using a JEM 200CX) of thin foils. Thinning of the foils was performed at 10 V in a solution of 70 ml ethanol, 10 ml glycerol and 20 ml perchloric acid at room temperature.

The as-cast structure was considerably modified by solid-state transformation. Careful metallographic examination was then necessary to deduce the previous structure at the early stages of the cooling process.

3. Results

All the phases occurring during the solidification process are indicated in the order of their appearance. Their transformation temperatures, determined from the DTA experiments, are reported in Table II. In the last column we have indicated the phases whose formation might occur during the cooling process. Fig. 1 illustrates the position of the different compositions plotted on Jackson's phase diagram [8] for Fe–Cr–C. In addition, the three typical thermograms exhibited by all the alloys are shown; they enable us to discriminate between three series of alloys according to their solidification paths. Alloys A, B, and C constitute the first family, their solidification phases appear in the following order: gamma-austenite, then M_7C_3-gamma eutectic and finally another carbide M_6C. Alloys D and H represent the second family whose solidification sequence is: delta-ferrite, then gamma-austenite then, again, M_7C_3-gamma eutectic. For the third family, which includes alloys E, F and G, the phases are the same in a different order: gamma-austenite followed by delta-ferrite and then M_7C_3-gamma eutectic. The results concerning each family are examined successively.

3.1. Family I – Alloys A, B and C

Our present investigation is limited to compositions close to the peritectic line alpha-

TABLE II Transformation temperatures and phases identified in order of formation during solidification

Alloy	Transformation temperatures (°C)	Phases formed during the solidification process	Phases formed during the cooling process
A	1388, 1257	γ, M_7C_3	
B	1371, 1217, 1147	γ, M_7C_3, M_6C	M_6C, M
C	1379, 1233, 1144	γ, M_7C_3, M_6C	M_6C, M
D	1421, 1355, 1288	δ, γ, M_7C_3	M_7C_3
E	1441, 1368, 1217, 1212	γ, δ, M_7C_3, Fe_2MoC	M_6C, Mo_2C, α, M
E*	1429, 1311, 1208, 1210	γ, δ, M_7C_3, Fe_2MoC	M_6C, α, M
F	1395, 1378, 1210, 1128	γ, δ, M_7C_3, M_6C	M_6C, Mo_2C, α, M
F*	1382, 1198, 1123	γ, M_7C_3, M_6C	M_6C, M
G	1454, 1384, 1246, 1124	γ, δ, M_7C_3, Fe_2MoC	M_6C, Mo_2C, α, M
H	1438, 1277	δ, M_7C_3	–

gamma in Jackson's phase diagram (Fig. 1). This kind of alloy has been more extensively studied in previous works [3]. The solidification sequence is not affected by small additions of manganese or silicon; these latter induce only slight decreases of the transformation temperatures. On the other hand addition of molybdenum promotes the formation of M_6C carbide in another step of crystallization revealed by a supplemental peak on the thermogram.

In the case of molybdenum alloys, slow cooling rates induce the formation of very fine precipitation located preferentially on the border of the grain (Fig. 2). The precipitates have been identified as M_6C type. They develop coherently with the matrix with an orientation relationship close to the classical cube–cube orientation, the value of the misorientation being about 5°.

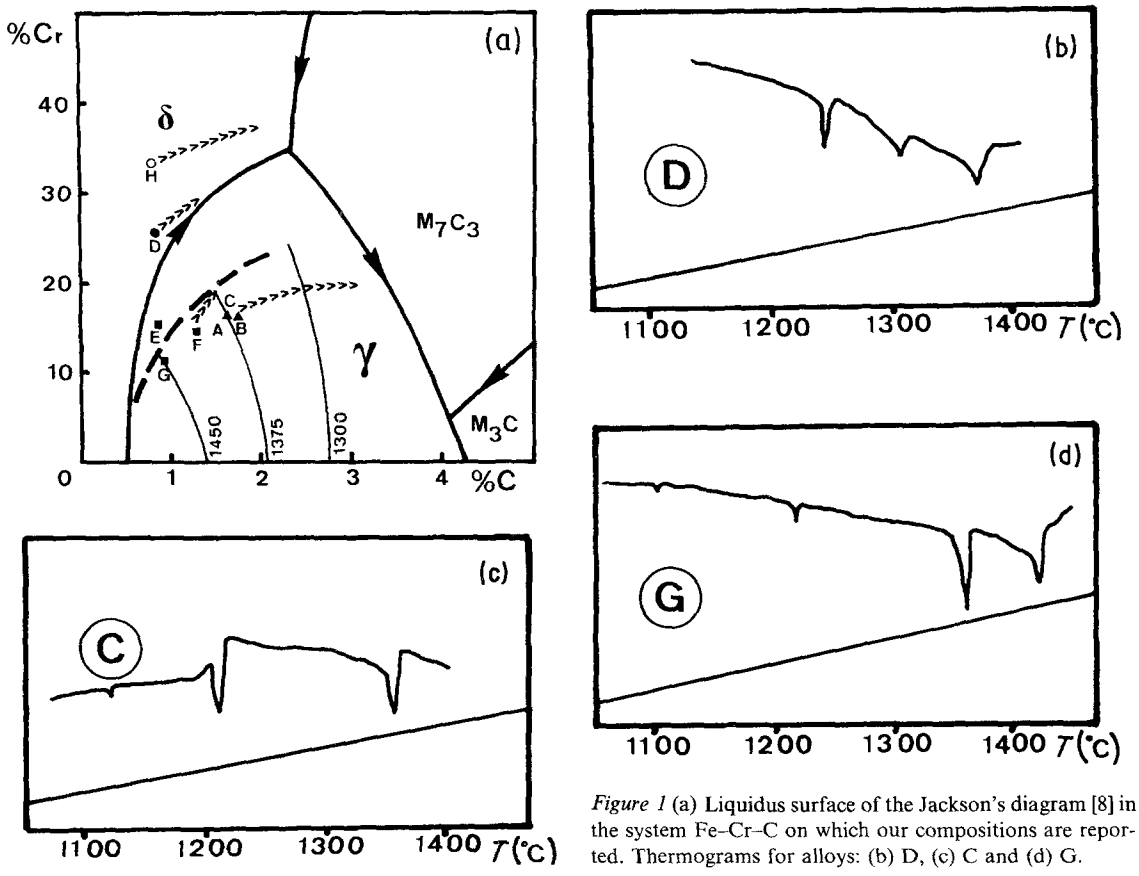

Figure 1 (a) Liquidus surface of the Jackson's diagram [8] in the system Fe–Cr–C on which our compositions are reported. Thermograms for alloys: (b) D, (c) C and (d) G.

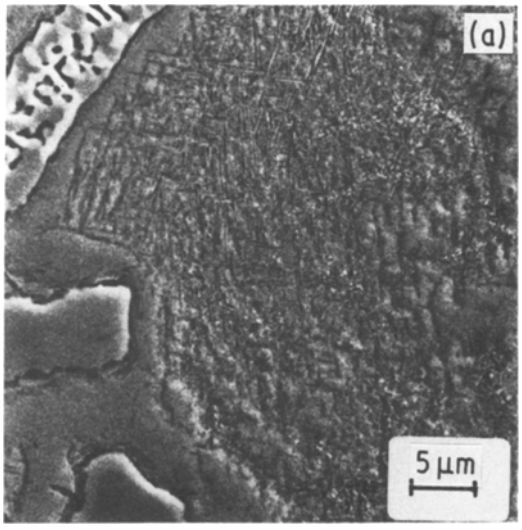

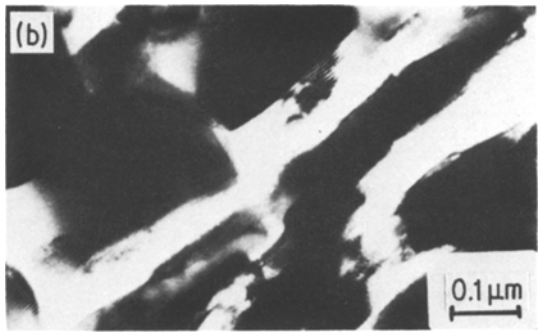

Figure 2 Secondary precipitation (a) secondary electrons (MEB) micrograph, (b) TEM micrograph, (c) key diagram of the diffraction pattern.

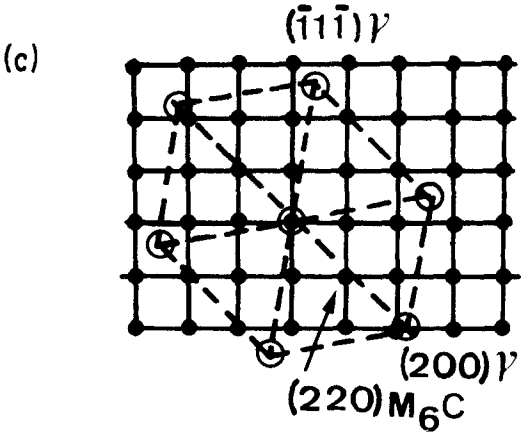

3.1. Family II – Alloys D, H

The primary crystallization is delta ferrite for both alloys, and Alloy D is the only one to exhibit also gamma-austenite. This is illustrated by the plots of crystallization paths on Fig. 1.

Fig. 3a shows the microstructure of alloy D corresponding to a slow cooling process. On the border line of the delta phase a precipitation of faceted carbides can be observed. They have been identified as M_7C_3 carbides and their composition is the same as the solidification carbides in the interdendritic groove. A string of these fine precipitates lies at the previous boundary between austenite and delta-ferrite. With a more accurate TEM observation we detected the transformation front surrounding the centre of the grain. It has not, however, been possible to observe any well defined orientation relationship between the M_7C_3 precipitates and their adjacent ferrite matrix.

3.3. Family III – Alloys E, F, G

The solidification begins by the formation of austenite as for the first family of alloys; then at high temperatures (a few degrees lower than the first liquidus temperature) another transformation occurs which is detected by the thermograms (Fig. 1). The second phase, located at the border of the dendrite, has been identified as ferrite, this is the common characteristic feature for this family. Depending on the cooling rate several types of solid-state transformation could then be observed.

The microstructure of Alloy E cooled at $600°C\,h^{-1}$ is shown in Fig. 3b. It exhibits a lamellar structure that we may call cellular since it consists of discontinuous cells of alternate lamellae. By TEM observations we identified austenite and M_6C carbides. These carbides are coherent with the matrix, and lie along preferential directions, the corresponding planes of the two lattices being approximately parallel. Fig. 4 presents all the TEM results. For higher cooling rates the transformed structure is very complex, and similar to the one which will be analysed in the following paragraph.

Alloy G has the composition of one of a series of molybdenum cast-irons which have been studied previously [3]. Very complex precipitation takes place depending on the cooling rate. It has been shown that martensitic plates embedded in austenite can be observed in the centre of the dendrite. The interdendritic grooves are made up essentially of austenite–carbide eutectic and between this structure and the dendritic austenite there is a dark, optically unresolvable border which corresponds to the previously solidified delta-ferrite. SEM micro-

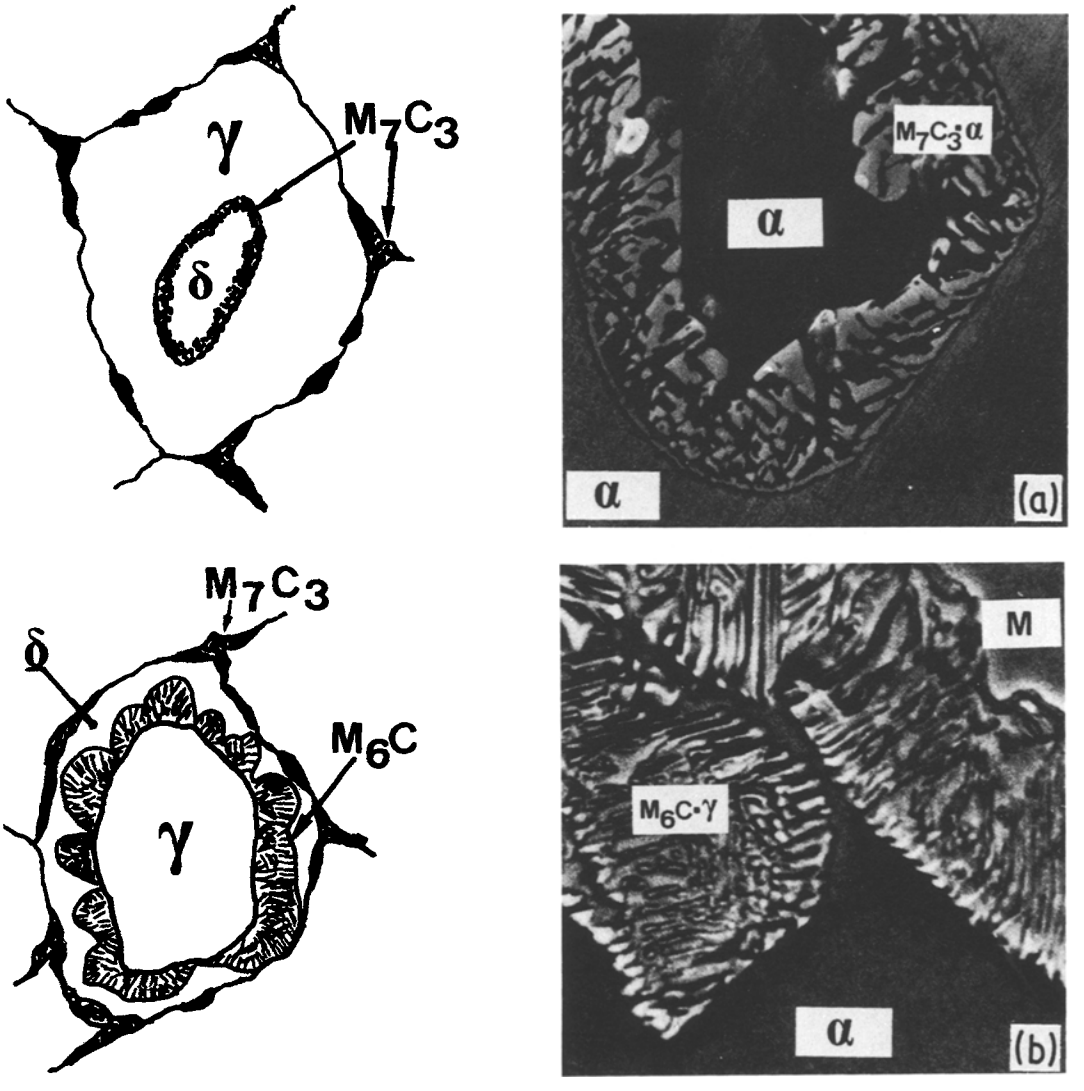

Figure 3 Discontinuous precipitation (a) MEB micrograph for alloy D cooled at 150° C h^{-1}, (b) MEB micrograph for alloy E cooled at 600° C h^{-1}. On the micrographs are indicated the phases identified at room temperature; on the schematics the phases as they are formed during the solidification process.

graphs in Fig. 5 show such zones at high magnification. The characteristic features of this zone is the occurrence of intricate lines. For Alloy F this zone does not constitute all the border; here, adjacent to the austenite, a zone of continuous precipitation has been observed (similar to that of Family I).

SEM and TEM investigations have been performed (see Fig. 6), which reveal intense and fine precipitation. The precipitates lie in rows, 0.5 to 1 μm long, aligned in specific directions. They are formed, in fact, by tiny cuboid precipitates orientated at 45° from the main direction. Diffraction patterns from this area enable them to be identified as Mo_2C within a ferritic phase (Fig. 6c). Some other block-like precipitates have been identified as M_6C with austenite (Fig. 6b). Four phases coexist in this alloy. The orientation relationship between ferrite and austenite was found to be the usual Nishiyama–Wasserman relationship, but no interface could be observed between these two phases.

The orientation relationships between M_6C and austenite are classic, as we have found for Family I. For Mo_2C in ferrite they are:

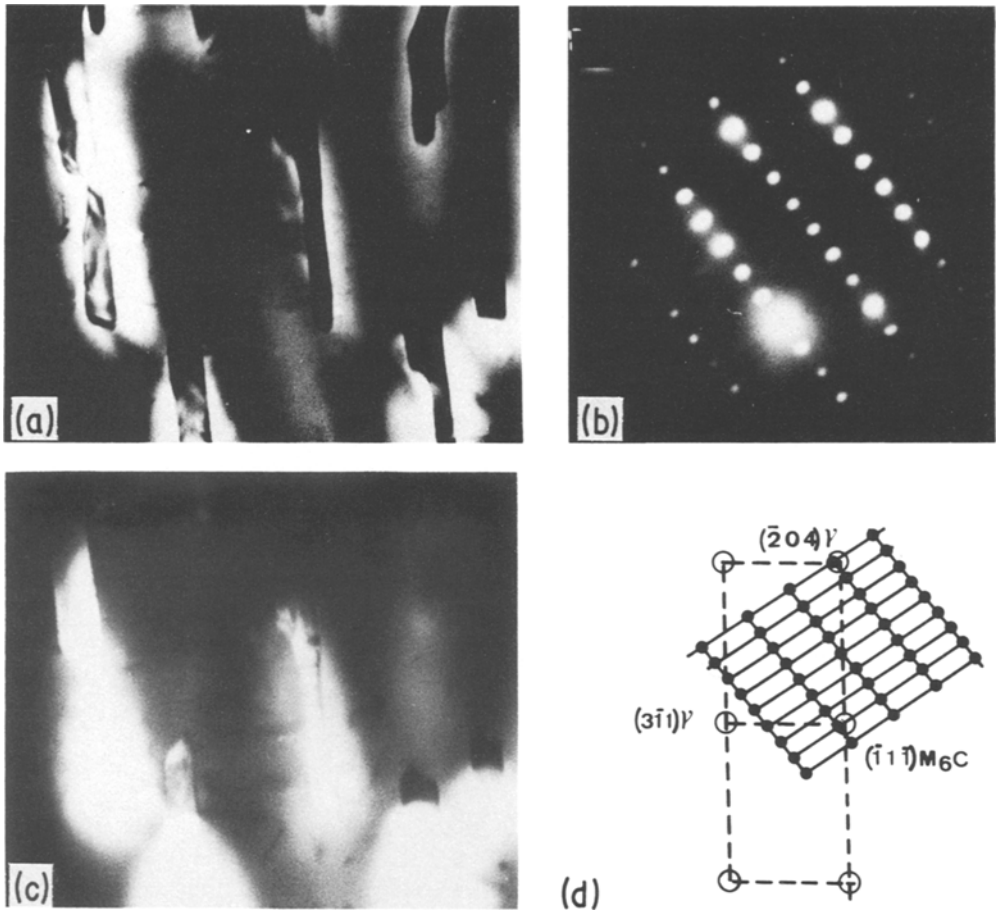

Figure 4 Lamellar structure of delta-pearlite in alloy E (a) MET micrograph, bright-field, (b) diffraction pattern, (c) key diagram and (d) MET micrograph, dark-field.

$$(0\,0.1)Mo_2C \parallel (0\,0\,1)F$$

$$[1\,2.0]Mo_2C \parallel [1\,1\,1]F$$

This orientation between Mo_2C and ferrite is different from the usual Pisch relationship [9], but it is identical to that postulated by Jack [10] for epsilon carbides (which have the same crystallographic structure as Mo_2C) in martensite. An important observation is that the ferrite is present as thin platelets which are

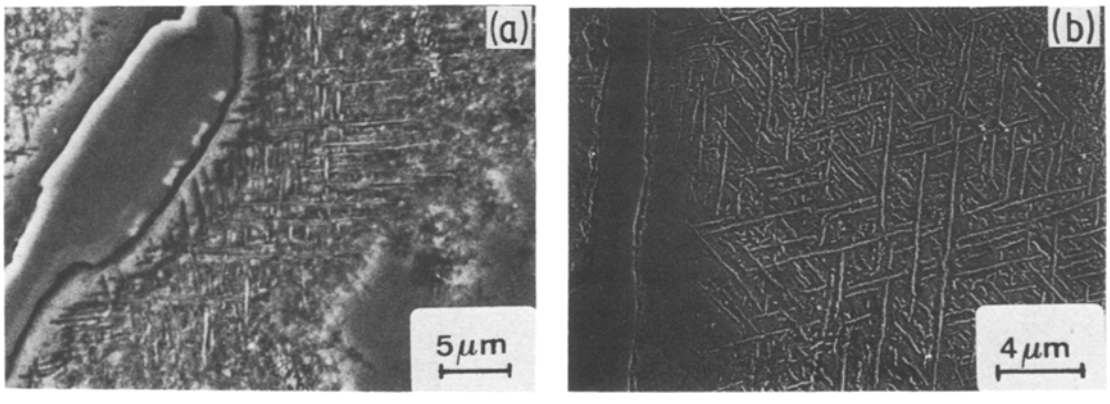

Figure 5 Precipitation in the ferritic border – MEB micrographs (a) alloy F cooled at 150° C h^{-1}, (b) alloy G cooled at 150° C h^{-1}

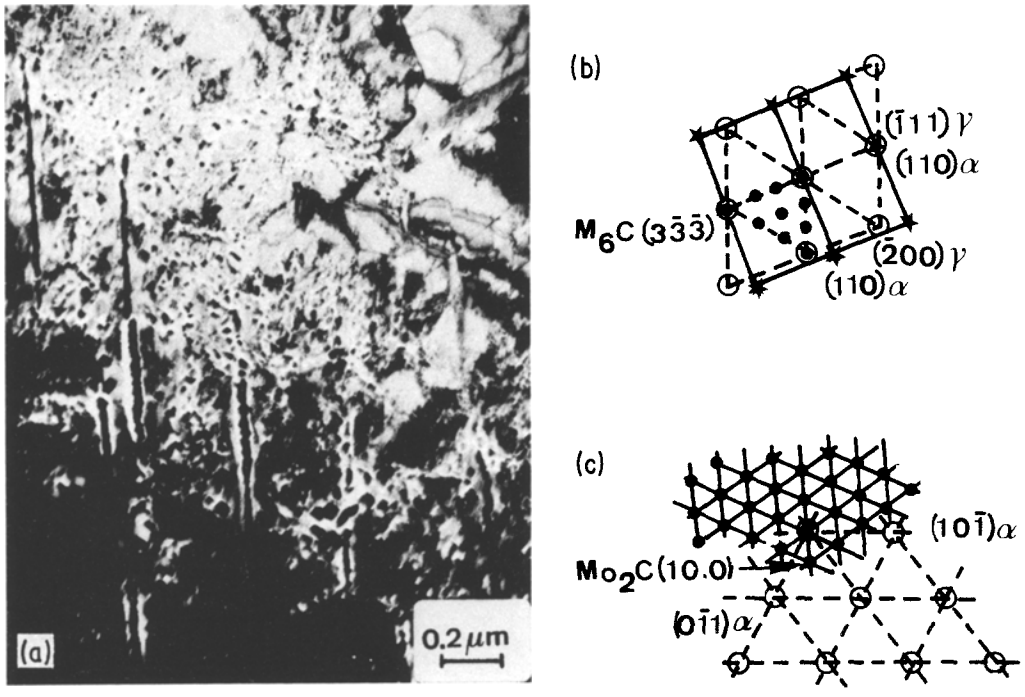

Figure 6 Precipitation in the ferritic border for alloy G (a) MET micrograph, (b) key diagram of the diffraction pattern for a (0 0 1) orientation of the thin foil, (c) key diagram of the diffraction pattern for a (1 1 1) orientation of the thin foil.

crystallographically oriented with respect to the austenite. This can be clearly seen in Fig. 6a where the ferrite contains rows of precipitates of Mo_2C. Quenching from temperatures of 900 to 950° C produces some similar ferrite platelets in austenite but here the precipitation does not occur.

Microhardness measurements have been performed on all these typical areas. Continuous precipitation (Family I) does not increase microhardness significantly. For the lamellar eutectoid precipitates microhardness values close to 320 uHv100 are observed while in the four-phased area an unexpectedly high hardness is developed (840 uHv100).

4. Discussion and conclusions

The first issue for discussion is the influence of the rate of solidification upon the crystallization paths and the corresponding temperatures. It is well known that the DTA results are not independent of the cooling rate and for high cooling rates such as $600° C h^{-1}$ a kinetic effect must be taken into account. Furthermore during the solidification time, back diffusion in the solid occurs to a greater or lesser extent according to the diffusion time; consequently the crystallization paths are different. The proportion of austenite and ferrite may therefore be slightly different.

The main effect related to the kinetics of the cooling process is the occurrence of many different solid-state transformations. We distinguished four types of such transformation:

(a) solid-state secondary precipitation
(b) cellular precipitation
(c) delta eutectoid transformation
(d) plate formation followed by two further precipitation reactions.

The secondary precipitation has been already described and discussed in a previous study concerning molybdenum cast-irons [3]. We should only point out here that the small M_6C carbide precipitates are coherent with the austenitic matrix and their orientation relationships are close to cube–cube. The formation of precipitates takes place mainly on the border of the grain because of solidification segregation and also on account of the partial dissolution of eutectic complex carbides.

Cellular precipitation is a well known mechanism involving the duplex growth of two phases in an alternating lamellar structure. In

the case of Alloy D our purpose is to point out the characteristic features which may be attributed to cellular growth.

As was the case with Alloy H, Alloy D displays delta-ferrite at the beginning of the solidification. Nevertheless the segregation of carbon in the liquid phase during the solidification process, induces the formation of austenite at the border of the dendrite since the increase of carbon and other austenite forming elements such as nickel extend the gamma loop [11]. At high temperature when the alloy has completely solidified there are, adjacent to one another, a ferritic phase and an austenitic phase. The partitioning of alloying elements results in a higher molybdenum and chromium content in the ferritic phase as has been indicated by several authors [12–14] and a higher carbon content in the austenitic phase. As the diffusivity of carbon is very important and still much more important than the diffusivity of carbide-forming elements chromium and molybdenum, the growth of carbides occurs in the ferritic phase. The first stage is the nucleation of precipitates at the delta–gamma grain boundary. They develop as a string of fine precipitates. Ainsley *et al.* [15] have explained the mechanism: in effect the discontinuous reaction begins with the precipitation of fine particles and this continues until part of the boundary is able to adopt a low-energy planar configuration in which there is a comparatively high density of coincident atoms in the boundary plane. When the boundary adopts such an orientation, a transition to the fibrous mode of growth takes place. It is worth noting that in this case, discontinuous precipitation produces either long fibres or faceted blocky carbides looking like the carbide primary dendrite growing from the liquid. Carbon consumed by the reaction is dragged from austenite, and this explains why the latter does not undergo martensitic transformation or secondary precipitation during further cooling. In fact austenite is transformed into ferrite after crossing the gamma loop, the ferrite can be readily identified in specimens at room temperature.

It is important to avoid confusion between the above continuous reaction which can be written:

$$\text{delta} \rightarrow \text{delta-prime} + M_7C_3$$

and an invariant precipitation reaction which results in the formation of very similar microstructure. This latter reaction can be written:

$$\text{delta} \rightarrow \text{gamma} + M_6C.$$

In the fifties a thorough investigation was carried out by Kuo [12, 13]. He has shown that delta-ferrite transforms at high temperature in austenite and M_6C carbides for high-speed steels containing tungsten. The microstructure displays alternating lamellae similar to those of pearlite; the lamellae are however coarser since the formation occurs at higher temperatures than for the pearlite. In the same manner as for cellular precipitation the transformation nucleates at the former delta-gamma interface. The presence of martensite is evidence for the prior austenite formation. Again the concentration of molybdenum and chromium is higher in the ferritic phase. The orientation relationship for this "delta-pearlite" is the same as for the secondary precipitation.

Turning lastly to the very complex microstructure illustrated by Alloy G (Fig. 6) we propose a mechanism involving several steps. The first one is the formation of austenite within delta-ferrite. It has been remarked that austenite often precipitates as a network at the ferrite grain boundary and as laths in a Widmanstätten structure [11]. Milanocha [16] mentioned a Widmanstätten structure in a maraging steel containing 2% molybdenum. By examination of the phase diagrams available in the literature, it appears that the systems containing molybdenum are more likely to provide a two-phase domain between delta and gamma [17]. Other similar systems involve the precipitation of carbides in the same range of temperatures. During the second stage of transformation each phase undergoes its own precipitation reaction. The orientation relationships have been discussed in our previous work [3]. In addition we should point out that the precipitation takes place within the laths and not at the grain boundary. It can be compared to the formation of epsilon carbides in martensite. In effect Simon [18] has established that the latter nucleate on microtwins in the middle of the lath. Adda *et al.* [19] have located the nucleation of epsilon carbides in twins or dislocations of the lath. In the same manner we can explain the nucleation of Mo_2C in the delta-ferrite; it is in good agreement with the fact that precipitates lie in lines in a lath.

The complex and diverse behaviour observed

in the present experiments provide an overall insight into the transformations exhibited by the high carbon alloyed steels. Care is needed in establishing structure–property relationships. The different segregating solutes can significantly modify the crystallization paths and may promote the formation of complex structures, the interpretation of which is often difficult.

References

1. K. ROHRIG, "Metallurgical aspects of wear" (Deustche Gesellschaft für Metallkunde, 1981) pp. 269–89.
2. J. D. B. DE MELLO, M. DURAND-CHARRE and T. MATHIA, *J. Mater. Sci. Eng.* Part I to be published.
3. J. D. B. DE MELLO, M. DURAND-CHARRE and S. HAMAR-THIBAULT, *Met. Trans.* **14A** (1983) 1793.
4. F. MARATRAY and R. USSELGIO-NANOT, "Atlas des courbes de transformation des fontes blanches au chrome et au chrome-molybdene" (Climax-Molybdenum France, 1970).
5. R. CASTRO and R. TRICOT, "Source Book on the ferritic stainless steels" (ASM Engineering bookshelf, 1982).
6. MARATRAY and POULALION, private communication (1983).
7. M. DURAND-CHARRE, B. CHOVELON, N. VALIGNAT and J. J. RAMEAU, *Mem. Sci. Rev. Metall.* (1980) 717.
8. R. S. JACKSON, *J. Iron Steel Inst.* **208** (1970) 153.
9. W. PISCH and A. SCHRADER, *Arch. Eisenhüttenw.* **29** (1958) 716.
10. K. H. JACK, *J. Iron Steel Inst.* **169** (1951) 26.
11. F. B. PICKERING, "Physical metallurgy and the design of steels", Materials Science (Applied Science Publishers).
12. K. KUO, *J. Iron Steel Inst.* (1954) 433.
13. *Idem, ibid.* (1955) 128.
14. H. FREDRICKSON, *Met. Sci.* **10** (1976) 77.
15. M. H. AINSLEY, G. J. COCKS and D. R. MILLER, *ibid.* **13** (1979) 20.
16. YA. N. MALINOCHKA, S. I. KRASNIKOVA, S. G. CHERNYAVSKAYA and N. E. PAVLENKO, *Metall. denie i Termicheskaya Obrabotka Metall.* **12** (1978) 28.
17. C. J. SMITHELLS, "Metals Reference Book" Vol. 1 (Butterworths, London, 1955).
18. A. SIMON, Thèse Docteur ès sciences Physique Université Nancy (1972).
19. Y. ADDA, J. M. DUPOUY, J. M. PHILIBERT and Y. QUERE, "Elements de Metallurgie Physique" (CEA Saclay 4, 30, 1978).

Received 25 June
and accepted 2 October 1984